SUPPLEMENTARY EXPERIMENTAL PROCEDURES

$CD34^+$ HSPC enrichment from cord blood.

$CD34^+$ HSPCs were enriched from freshly processed cord blood samples by magnetic separation using CD34 microbeads (Miltenyi Biotech) per manufacturer's protocol and cultured in HPGM medium (Lonza) supplemented with FLT3 ligand, thrombopoietin, and stem cell factor. The cytokines were all purchased from Peprotech and used at 20 ng/ml final concentration.

Construction of cDNA expression lentiviral vectors.

The complementary DNA (cDNA) clones of human RAD21 (Accession: BC001229), SMC3 (Accession: BC047324) and STAG2 (Accession: BC017095) were purchased from GE Healthcare Dharmacon in the pCMV-SPORT6 vector. SMC1A (Accession: BC112127) was purchased in pCR-XL-TOPO. The mutations presented in this paper (RAD21 E212*, RAD21 Q592*, SMC1A R711G, SMC3 G662C and STAG2 Q801*) were generated using the QuikChange II site-directed mutagenesis kit (Agilent Technologies) per manufacturer's instructions. The open reading frames of wild-type or mutant RAD21/SMC1A/SMC3/STAG2 were PCR amplified and cloned into the pLVX-EF1a-IRES-zsGREEN vector (Clontech) and doxycycline-inducible pINDUCER21 (IRES-eGFP) from the Elledge Lab (Addgene plasmid #46948) using the Infusion Cloning Kit per manufacturer's instructions (Clontech).

Construction of shRNA expression lentiviral vectors.

The human RAD21 (Accession: BC001229), GATA1 (Accession: NM_002049.3), GATA2 (Accession: NM_001145661.1), PU.1 (Accession: NM_001243998.1) and RUNX1 (Accession: NM_001001890.2) shRNA target sequences (**Table S4**) were selected using the BLOCK-iT RNAi Designer tool (Life Technologies). Cloning into pRSI9 DECIPHER shRNA expression vector (Cellecta) was conducted as previously described (Chan et al., 2015). Knockdown efficiency of shRNA constructs was determined using qRT-PCR using Taqman assays from Life Technology (see **Gene Expression Assays**). The scramble control sequence used in this study was 5′-GCACTACCAGAGCTAACTCAGATAGTACT-3′.

Lentivirus production.

The 293TN producer cell line (System Biosciences) was grown in Advanced DMEM (Life Technologies) with 10% FBS and 2 mM GlutaMAX. One day before transfection, 4 million cells were plated in a 150-mm tissue-culture dish. On the day of transfection, 13.5 μg of the lentiviral expression plasmid was combined with 8.8 μg of the packaging vector psPAX2 and 4.7 μg of the envelope expressing plasmid pCMV-VSV-G. The DNA mixture was diluted in Opti-MEM I medium (Life Technologies), mixed with 293fectin transfection reagent (Life Technologies) at a ratio of 3 μl per 1 μg of DNA and added to the plated 293TN cells. Viral supernatant was collected at 72 h after transfection, filtered through a 0.45-μm PVDF filter and concentrated via ultracentrifugation at 23,000rpm for 2 hours. The concentrated lentiviral particles were resuspended in HBSS with 25 mM HEPES and stored at −80 °C.

Gene Expression Assays.

Quantitative real-time PCR (qRT-PCR) was performed as previously described (Reinisch et al., 2015). Taqman gene expression assays were purchased from Life Technologies: RAD21 (Hs00366721_mH), SMC1A (Hs00196849_m1), SMC3 (Hs00271322_m1), STAG2 (Hs00198227_m1), GATA1 (Hs01085823_m1), GATA2 (Hs00231119_m1), GATA3 (Hs00231122_m1), PU.1 (Hs00162150_m1), ERG (Hs01554629_m1), RUNX1 (Hs01021970_m1), KLF-1 (Hs00610592_m1), HBG1/2 (Hs00361131_g1)

Cell Proliferation Assay

To assess the proliferation of cells we used Absolute Countbright beads (Life Technology) as per manufacturer protocol.

THP-1 Differentiation Assays

THP-1 cells were induced with DOX for 48 hours and then differentiation was induced with all-trans retinoic acid at 1 uM as previously described (Drach et al., 1993). Macrophage differentiation was monitored by surface expression of anti-human CD11b-PE-Cy5 (ICRF44) (BD Biosciences).

THP-1 cells were induced with DOX for 48 hours and then differentiation was induced with phorbol 12-myristate 13-acetate (PMA) at a concentration of 100 ng/mL for 48 hours as

previously described (Park et al., 2007). Macrophage differentiation was monitored by surface expression of anti-human CD11b-PE-Cy5 (ICRF44) (BD Biosciences).

Annexin V staining.

Staining for apoptotic cells was performed as previously described (Chan et al., 2015).

HSPC Subpopulation Sorting

A previously established panel of antibodies was used for analysis and sorting of hematopoietic stem and progenitor populations (Majeti et al., 2007). Briefly, mononuclear cells were isolated from freshly processed UCB by density gradient centrifugation (Ficoll, GE Healthcare). Thereafter, CD34+ cells were pre-enriched using MACS-technology (Miltenyi), washed, and incubated for 30 minutes, at 4ºC with monoclonal anti CD2 (RPA-2.10), CD3 (S4.1), CD4 (S3.5), CD7 (CD7-6B7); CD8 (3B5), CD11b (ICRF44), CD14 (TUK4), CD16 (3GA), CD19 (SJ25-C1), CD20 (13.6E12), CD56 (B159), GPA (GA-R2, all PE-Cy5, all BD), as well as CD45RA-BV605 (MEM56, ebioscience), CD10-APC-Cy7 (HI10a, biolegend), CD90-FITC (5E10), CD123-PE (7G3), CD38-PE-Cy7 (HIT2), CD34-APC (8G12, all BD) antibodies.

Western blotting.

Standard western blotting and co-immunoprecipitation techniques were performed. A rabbit monoclonal RAD21 antibody (clone D5Y8S; Cell Signaling) was used at a dilution of 1:1,000. A goat polyclonal antibody against SMC1A (Abcam) was used at a dilution of 1:1,000. A rabbit monoclonal antibody against SMC3 (clone D47B5, Cell Signaling) was used at a dilution of 1:2,000. A mouse monoclonal β-actin antibody (clone 8H10D10; Cell Signaling) was used at a dilution of 1:5,000. Standard secondary antibodies conjugated to HRP were used following incubation with primary antibodies. Cell lysis for western blotting and co-immunoprecipitation was conducted as previously described (Kon et al., 2013).

Intracellular flow cytometry staining.

Intracellular staining of TF-1 cells was conducted per Cell Signaling's online protocol using a phospho-gamma-H2AX antibody (Clone 20E3) conjugated to Alexa-647 (Cell Signaling) at a dilution of 1:100. A rabbit IgG isotype control antibody conjugated to Alexa Fluor-647 was used to determine background nonspecific fluorescence staining.

ATAC-Seq Analysis

Data preprocessing

ATAC-Seq paired end reads were trimmed for Illumina adapter sequences and transposase sequences using an in-house script and mapped to hg19 using Bowtie v0.12.9 (Langmead et al., 2009) with parameters –S –X2000 –m1. Duplicate reads were discarded with Samtools v0.1.18 (Li et al., 2009). Peak calling using ZINBA was as described (Rashid et al., 2011). Chromosomal regions with a posterior probability of >0.99 were identified as peaks. Overlapping peaks from all samples were merged together to a unique peak list, and number of raw reads mapped to each peak for each individual samples was quantified.

Differential Analysis and Motif Analysis of ATAC-Seq peak

Differentially accessible peaks from the union peak list were identified with edgeR (Robinson et al., 2009) using raw counts of each sample in the overlapping peak list. edgeR was run with default settings, with a fold change threshold of 2, and P-value < 0.01. Motif analysis was performed using HOMER (http://homer.salk.edu/homer/motif/) with default parameters to test the occurrence of a TF motif in peaks regions compared to that in background regions.

ATAC-Seq signal intensity around TSS

A 1kb window centered on TSS was divided into twenty 50 equal sized bins. The number of unique-mapped and properly paired ATAC-Seq tags overlapping each bin was counted. The average fragment count plotted in each bin was normalized to the average tag count in the first five bins in order to normalize the background signal among various samples. The heat maps of ATAC-Seq at all the TSS regions were generated using Java TreeView 3.0.

V-plot analysis for nucleosome positioning

V-plots for cohesin WT (RAD21WT, SMC1A WT) and cohesin mutants (RAD21 mutants, SMC1A mutants) were normalized by sequencing depth, which allows for direct visual comparison of nucleosome position near TSS region (1 kb window; 500 bp left and 500 bp right). The X-axis represents the distance between the mid-point of the fragments to TSS. The Y-axis represents the fragment length. The color represents the intensity of ATAC-Seq (the number of fragments at the coordinates).

PIQ Footprinting Analysis

The genome-wide motif footprinting analysis was performed using PIQ v1.3 (Sherwood et al., 2014) with input motif position weight matrices (PWM) from jasper database (http://jaspar.genereg.net/). For footprinting, we adjusted the read start sites to represent the center of the transposon binding event. Previous studies of the Tn5 transposase have shown that the transposon binds as a dimer and inserts two adaptors separated by 9 bp (Adey et al., 2010). Therefore, all reads mapped to the forward strand were offset by +4 bp, and all reads mapped to the reverse strand were offset -5 bp. The purity scores (indicating the likelihood of true TF binding) from PIQ algorithm were compared between cohesin WT and mutant samples by paired t-test.

ChIP-Seq Analysis

ChIP-seq single end reads were mapped to hg19 using Bowtie2 v2.1.0 (Langmead and Salzberg, 2012) with–very sensitive option. Peaks were identified using MACS2 (Zhang et al., 2008) with default parameters. The differential binding of transcription factors between ChIP-Seq samples were identified using MAnorm (Shao et al., 2012). The average diagram ChIP-Seq signal (GATA2 and RUNX1) of ChIP-Seq signal around 1kb of the TF motif in 50 bp resolution was plotted using an in-house script.

shRNA Primers	
RAD21 shRNA #1 –Fwd	ACCGGCAGCTTATAATGCCATTATCAAGAGTAATGGCATTATAAGCTGCTTTT
RAD21 shRNA #1 –Rev	CGAAAAAAGCAGCTTATAATGCCATTACTCTTGATAATGGCATTATAAGCTGC
RAD21 shRNA #2 –Fwd	ACCGGCCACTGCCTGACTTAGATTCAAGAGATCTAAGTCAGGCAGTGGCTTTT
RAD21 shRNA #2 –Rev	CGAAAAAAGCCACTGCCTGACTTAGATCTCTTGAATCTAAGTCAGGCAGTGGC
GATA1 shRNA #1 –Fwd	ACCGGCCTCTATCACAAGATGAATGTCAAGAGCATTCATCTTGTGATAGAGGCTTTT
GATA1 shRNA #1 –Rev	CGAAAAAAGCCTCTATCACAAGATGAATGCTCTTGACATTCATCTTGTGATAGAGGC
GATA1 shRNA #2 –Fwd	ACCGGCGCCTGATTGTCAGTAAACGTCAAGAGCGTTTACTGACAATCAGGCGCTTTT
GATA1 shRNA #2 – Rev	CGAAAAAAGCGCCTGATTGTCAGTAAACGCTCTTGACGTTTACTGACAATCAGGCGC
GATA2 shRNA #1 –Fwd	ACCGGGAACCGGAAGATGTCCAACATCAAGAGTGTTGGACATCTTCCGGTTCCTTTT
GATA2 shRNA #1 – Rev	CGAAAAAAGGAACCGGAAGATGTCCAACACTCTTGATGTTGGACATCTTCCGGTTCC
GATA2 shRNA #2 –Fwd	ACCGGGTGGACGTCTTCTTCAATCATCAAGAGTGATTGAAGAAGACGTCCACCTTTT
GATA2 shRNA #2 – Rev	CGAAAAAAGGTGGACGTCTTCTTCAATCACTCTTGATGATTGAAGAAGACGTCCACC
PU.1 shRNA #1 – Fwd	ACCGGCTTCGCCGAGAACAACTTCATCAAGAGTGAAGTTGTTCTCGGCGAAGCTTTT
PU.1 shRNA #1 – Rev	CGAAAAAAGCTTCGCCGAGAACAACTTCACTCTTGATGAAGTTGTTCTCGGCGAAGC
PU.1 shRNA #2 – Fwd	ACCGGCAAGAAGATGACCTACCAGATCAAGAGTCTGGTAGGTCATCTTCTTGCTTTT
PU.1 shRNA #2 – Rev	CGAAAAAAGCAAGAAGATGACCTACCAGACTCTTGATCTGGTAGGTCATCTTCTTGC
RUNX1 shRNA #1 –Fwd	ACCGGGATACAAGGCAGATCCAACCTCAAGAGGGTTGGATCTGCCTTGTATCCTTTT
RUNX1 shRNA #1 – Rev	CGAAAAAAGGATACAAGGCAGATCCAACCCTCTTGAGGTTGGATCTGCCTTGTATCC
RUNX1 shRNA #2 –Fwd	ACCGGGCTGAGCTGAGAAATGCTACTCAAGAGGTAGCATTTCTCAGCTCAGCCTTTT
RUNX1 shRNA #2 – Rev	CGAAAAAAGGCTGAGCTGAGAAATGCTACCTCTTGAGTAGCATTTCTCAGCTCAGCC
ERG shRNA #1 – Fwd	ACCGGCACTATTAAGGAAGCCTTATTCAAGAGATAAGGCTTCCTTAATAGTGCTTTT
ERG shRNA #1 – Rev	CGAAAAAAGCACTATTAAGGAAGCCTTATCTCTTGAATAAGGCTTCCTTAATAGTGC
ERG shRNA #2 – Fwd	ACCGGGAGTGGGCGGTGAAAGAATATCAAGAGTATTCTTTCACCGCCCACTCCTTTT
ERG shRNA #2 – Rev	CGAAAAAAGGAGTGGGCGGTGAAAGAATACTCTTGATATTCTTTCACCGCCCACTCC

SUPPLEMENTARY FIGURE AND TABLE LEGENDS

Figure S1. Cohesin Mutants Exhibit no Changes in Proliferation, Apoptosis or DNA Damage, Related to Figure 1.

(A) TF-1 cells were infected with lentiviruses encoding doxycycline (DOX)-inducible cohesin WT or mutant variants and green fluorescent protein (GFP). After 6 days of DOX induction, expression of cohesin complex genes (RAD21, SMC1A, SMC3, and STAG2) was determined by qRT-PCR. Values normalized to TF-1 No DOX control.

(B) Whole cell lysate Western blot analysis of cohesin component expression from TF-1 cell lines after 6 days of DOX induction. Anti-RAD21, anti-SMC1A, anti-SMC1A, and anti-STAG2 antibodies were used, and beta-actin was monitored as a protein loading control. Cohesin mutant samples are bolded.

(C) THP-1 cells were infected with lentiviruses encoding doxycycline (DOX)-inducible cohesin WT or mutant variants and green fluorescent protein (GFP). Myeloid differentiation of parental THP-1 cells and variants was determined by flow cytometry for CD11b expression after 2 initial days of DOX treatment and 4 days of 1uM all trans retinoic acid (ATRA). Relative expression shown as mean fluorescence intensity (MFI) of CD11b normalized to IgG isotype control. * indicates $p<0.05$ and ** indicates $p<0.01$.

(D) THP-1 lentivirally transduced as in (C) were induced to differentiate with 100 ng/mL phorbol myristate acetate (PMA). Myeloid differentiation of parental THP-1 cells and variants was determined by flow cytometry for CD11b expression after 2 initial days of DOX treatment and 4 days of PMA. Relative expression shown as mean fluorescence intensity (MFI) of CD11b normalized to IgG isotype control. ** indicates $p<0.01$.

(E) TF-1 cells were infected with lentiviruses encoding doxycycline (DOX)-inducible cohesin WT or mutant variants and green fluorescent protein (GFP). Proliferation by absolute cell count (trypan blue exclusion) after 2 initial days of DOX treatment was monitored every 4 days for a total of 20 days. No statistically significant differences were detected.

(F) TF-1 cells treated as in (E) were analyzed after 8 days in culture following DOX induction for Annexin V positivity and propidium iodide (PI) staining by flow cytometry. % Annexin V (-) cells is shown. No statistically significant differences were detected.

(G) TF-1 cells treated as in (E) were cultured and then fixed and permeabilized for phospho-gamma H2AX intracellular staining after the 3 indicated time points. Relative expression is shown as mean fluorescence intensity (MFI) of phospho-gamma H2AX normalized to IgG isotype control. TF-1 cells treated with 1uM etoposide was used as a positive control for phospho-gamma H2AX staining. No statistically significant differences were detected.

Figure S2. Cohesin Mutants do not Affect Proliferation and Apoptosis of Primary Human HSPC , Related to Figure 2.

(A) Human CD34-enriched cord blood HSPC were infected with lentiviruses encoding GFP alone (control) or GFP in addition to the indicated cohesin variants. 72 hours post-infection, GFP+ cells were isolated by FACS and expression of cohesin complex genes (RAD21, SMC1A, SMC3, and STAG2) was determined by qRT-PCR. Values normalized to empty vector control.

(B) HSPC treated as in (A) were cultured in HSPC-retention medium. Proliferation was monitored using absolute countbright beads by flow cytometry. The proliferation rate was calculated by normalizing to non-transduced control. No statistically significant differences were detected.

(C) HSPC treated as in (A) were analyzed after 4 days for Annexin V positivity and propidium iodide (PI) staining by flow cytometry. %Annexin V (-) cells is shown. No statistically significant differences were detected.

(D) HSPC were infected with lentiviruses encoding GFP alone (control) or GFP in addition to the indicated cohesin variants. 72 hours post-infection, GFP(-) cells were isolated by FACS and cultured in HSPC-retention medium. 6 days later, cells were analyzed for expression of progenitor markers CD34 and CD38. Representative FACS plots are shown. No statistically significant differences were detected.

(E) HSPC isolated and lentivirally transduced as in (D) were cultured in myeloid differentiation medium. 6 days later, cells were analyzed for expression of myeloid markers CD33 and CD14. Representative FACS plots are shown. No statistically significant differences were detected.

(F) HSPC isolated and lentivirally transduced as in (D) were cultured in erythroid differentiation medium. 6 days later, cells were analyzed for expression of erythroid markers CD71 and GPA. Representative FACS plots are shown. No statistically significant differences were detected.

Figure S3. Knockdown of RAD21 Impairs Myeloid, Erythroid, and Stem Cell Differentiation of Primary Human HSPC, Related to Figure 3.

(A) RAD21 expression was determined by qRT-PCR to determine the knockdown efficiency of 3 RAD21 shRNA vectors including 1 inducible vector (#3) and 2 constitutive vectors (#1 and #2) in FACS-purified RFP+ CD34-enriched cord blood. Expression is reported relative to a scrambled shRNA control.

(B) RAD21 protein expression was determined by Western blot in TF-1 cells transduced with the same 3 RAD21 shRNA vectors. Cells transduced with inducible vector #3 were analyzed in the absence and presence of DOX. Beta-actin was monitored as a protein loading control.

(C) TF-1 cells were infected with lentiviruses encoding doxycycline (DOX)-inducible RAD21 shRNA or constitutive RAD21 shRNAs and FACS-sorted for GFP+ or RFP+ cells. Erythroid differentiation of the resulting cell lines was determined by qRT-PCR for fetal hemoglobin expression after 2 initial days of DOX treatment and 8 days of EPO and DOX treatment. Values normalized to TF-1 control. ** indicates $p<0.01$.

(D) Expression of KLF-1 was determined by qRT-PCR for cells treated as in (C). Values normalized to TF-1 controls. ** indicates $p<0.01$.

(E) Human CD34-enriched cord blood HSPC were infected with constitutive RAD21 shRNA or scramble control RFP-encoding lentiviral vectors. 72 hours post-infection, RFP+ cells were FACS-purified and cultured in HSPC-retention medium as in Figure 2. 6 days later, cells were analyzed for expression of progenitor markers CD34 and CD38. Representative FACS plots are shown.

(F) Summary of data from 3 independent experiments as described in (E); the percentage of CD34+ cells was normalized to scramble shRNA control. Unpaired Student t test was used to determine statistical significance between RAD21 WT and RAD21 knockdown and mutant-expressing populations. ** indicates $p<0.01$.

(G) HSPC isolated and lentivirally transduced as in (E) were cultured in myeloid differentiation medium. 6 days later, cells were analyzed for expression of myeloid markers CD33 and CD14. Representative FACS plots are shown.

(H) Summary of data from 3 independent experiments as described in (G); the percentage of CD33+/CD14+ cells was normalized to GFP control. Unpaired Student t test was used to determine statistical significance between WT and mutant populations. ** indicates $p<0.01$.

(I) HSPC isolated and lentivirally transduced as in (E) were cultured in erythroid differentiation medium. 6 days later, cells were analyzed for expression of erythroid markers CD71 and GPA. Representative FACS plots are shown.

(J) Summary of data from 3 independent experiments as described in (I); the percentage of GPA+/CD71+ cells was normalized to GFP control. Unpaired Student t test was used to determine statistical significance between WT and mutant populations. ** indicates $p<0.01$.

Figure S4. Primary Cohesin-Mutant AML Samples Exhibit Reduced Expression of Cohesin Components and Reduced Binding to Cohesin Partners, Related to Figure 4.

(A) Whole cell lysate Western blot analysis of cohesin component expression from 7 primary patient samples and 2 TF-1 cell line samples is shown. Anti-RAD21, anti-SMC3, and anti-SMC1A antibodies were used, and beta-actin was monitored as a protein loading control. Cohesin mutant samples are bolded.

(B) Co-immunoprecipitation analysis from samples shown in (A). Whole cell lysates were first immunoprecipitated using an anti-SMC1A antibody and then blotted with anti-RAD21, SMC3, or SMC1A antibodies.

Figure S5. Knockdown of RAD21 Impairs Human HSPC Differentiation in a Cell Context-Dependent Manner, Related to Figure 5.

(A) Representative FACS plots (pre-sort) and purity analysis (post-sort) for purification of HSPC subpopulations including: HSC, MPP, LMPP, CMP, GMP, and MEP.

(B) Human CD34-enriched cord blood was sorted for HSPC subpopulations (HSC, MPP, LMPP, CMP, MEP, and GMP). Each subpopulation was then transduced with

lentiviruses encoding scramble shRNA (RFP) or RAD21-shRNA (RFP). The virally transduced cells were cultured in myeloid differentiation medium, as in Figure 2. 8 days later, the cells were analyzed by flow cytometry for expression of myeloid markers CD33 and CD14. Representative FACS plots of RFP+ cells are shown of 3 independent experiments.

(C) HSPC subpopulations isolated and lentivirally transduced as in (B) were cultured in erythroid differentiation medium, as in Figure 2. 8 days later, the cells were analyzed for expression of erythroid markers CD71 and GPA. Representative FACS plots of RFP+ cells are shown of 3 independent experiments.

Figure S6. Cohesin Mutants Exhibit Decreased Chromatin Accessibility at K562 Promoter and Enhancer Features, Increased Expression of HSPC Transcription Factors, and Increased Binding of HSPC Transcription Factors at Open Chromatin Sites, Related to Figure 6.

(A) Human CD34-enriched HSPC were infected with control, cohesin WT, or cohesin mutant GFP-encoding lentiviruses. 3 days later, GFP+ transduced cells were FACS-purified and subject to ATAC-Seq. The heat map shows the Pearson correlation between every pair of the cohesin WT and mutant samples. A dendrogram from hierarchical clustering based on the Euclidean distance of the sample correlation vectors is shown symmetrically on the top and left sides of the heat map. The color bar (1 – correlation) on the left corner is ranged from 0 to 1.

(B) The heat map of ATAC-Seq signal intensity in 15 annotated genomic features. The genomic features are annotated based on ChromHMM states learned by histone markers of K562 cell line (ENCODE data). The ATAC-Seq signal intensity is indicated by the percentage of unique-mapped and properly-paired ATAC-Seq tags in each ChromHMM state. The data in each row of the heat map were standardized for contrast in visualization. The dendrogram on top of the heat map is based on a hierarchical clustering of genome-wide ATAC-Seq tag distribution of cohesin WT, cohesin mutants, normal CD34+ CD38-, and normal CD34+ CD38+ cells.

(C) HSPC isolated and lentivirally transduced as in (A) were subjected to qRT-PCR for expression of HSPC transcription factors (ERG, GATA2, and RUNX1). Freshly isolated

normal HSPC subpopulations (CD34+/CD38-, CD34+/CD38+, and Lineage +) were analyzed in parallel.

(D) TF-1 RAD21 WT and RAD21 Q592* were induced with DOX for 6 days and then subjected to ChIP-Seq for GATA2 and RUNX1. Average diagrams for ChIP-Seq signal at GATA2 and RUNX1 motifs shown here for all ATAC-Seq peaks differentially upregulated in RAD21-mutant HSPC.

(E) Illustrative tracks of ChIP-Seq signal (normalized to input) for GATA2, TAL1, and CD34 in TF-1 RAD21 WT vs. TF-1 RAD21 Q592* cells treated as in (D).

(F) Overlap of ChIP-Seq peaks of GATA2, RUNX1, or SMC3 with chromatin accessible sites that were gained or lost in RAD21 WT or RAD21 Q592* cells. Note that GATA2 and RUNX1 ChIP-seq peaks are enriched in accessible sites gained in cells expressing mutant RAD21.

Figure S7. Knockdown of GATA1 and PU.1 reduces erythroid and myeloid differentiation, respectively, Related to Figure 7.

(A) CD34-enriched cord blood HSPC were transduced with lentiviruses encoding scramble or transcription factor-targeting shRNAs and cultured in HSPC-retention medium. 6 days later, cells were analyzed for expression of progenitor markers CD34 and CD38. Representative FACS plots are shown of 3 independent experiments.

(B) HSPC isolated and lentivirally transduced as in (A) were cultured in erythroid differentiation medium. 6 days later, cells were analyzed for expression of erythroid markers CD71 and GPA. Representative FACS plots are shown of 3 independent experiments.

(C) HSPC isolated and lentivirally transduced as in (A) were cultured in myeloid differentiation medium. 6 days later, cells were analyzed for expression of myeloid markers CD33 and CD14. Representative FACS plots are shown of 3 independent experiments.

Table S1. Primary AML Sample Information, Related to Figure S4.

Table S2. Differentially Expressed Genes Between Cohesin Mutant and WT Cord Blood, Related to Figure 3.

Table S3. Top 50 Motifs Upregulated in ATAC-Seq Data, Related to Figure 6.

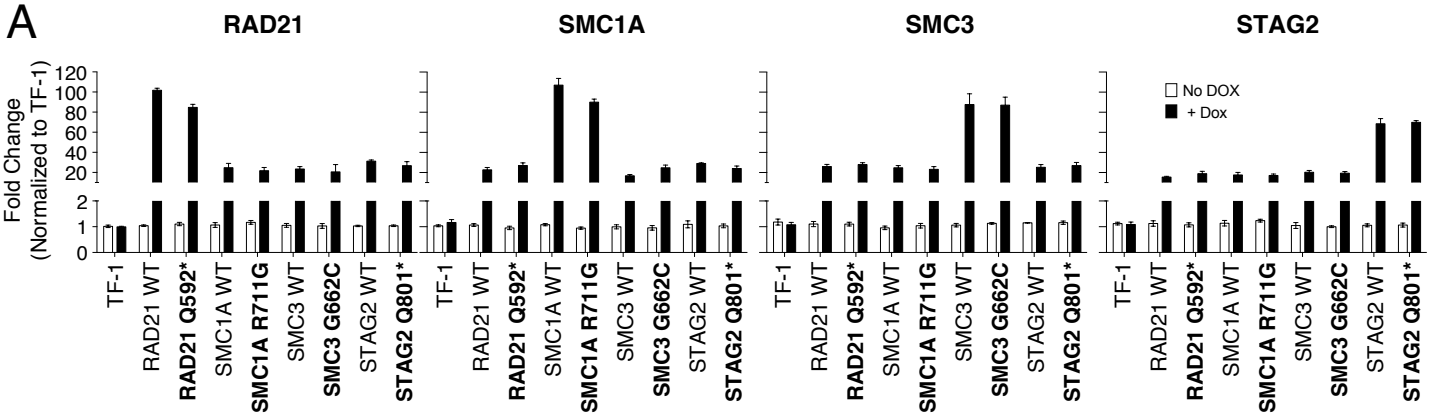

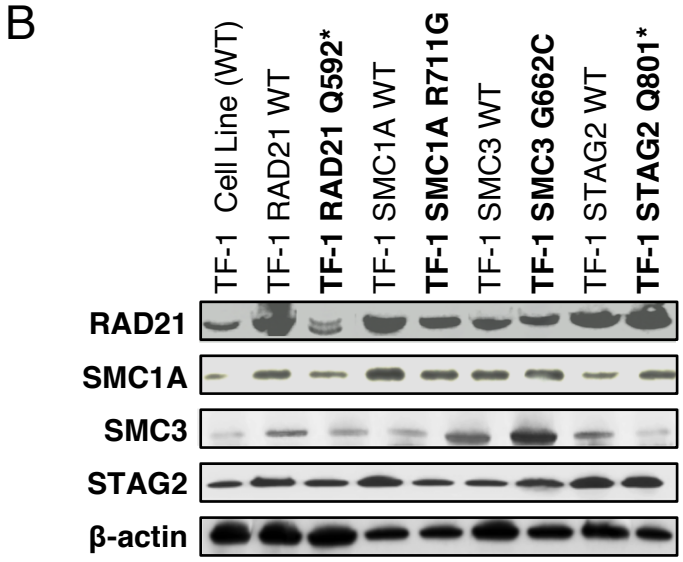

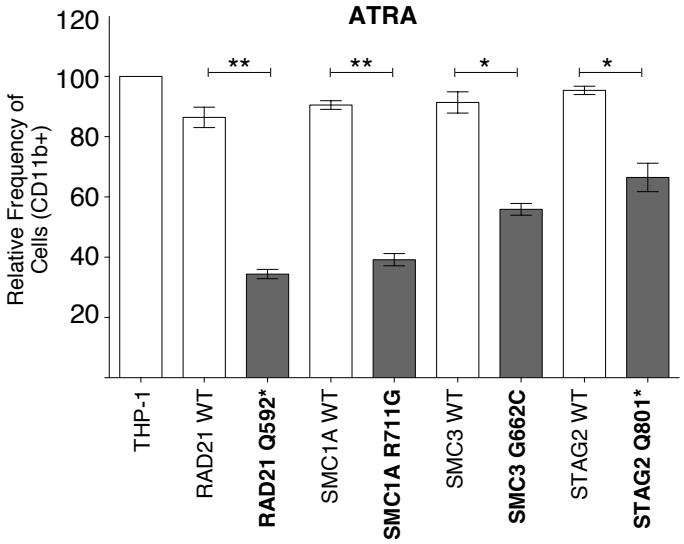

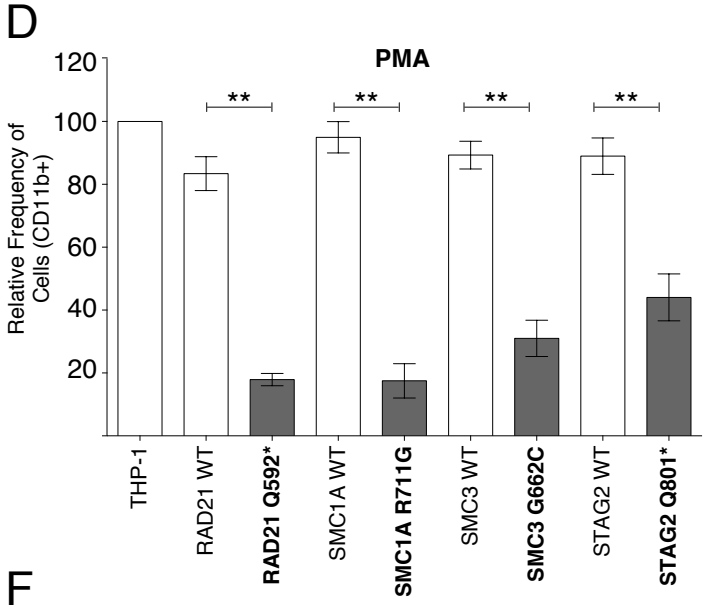

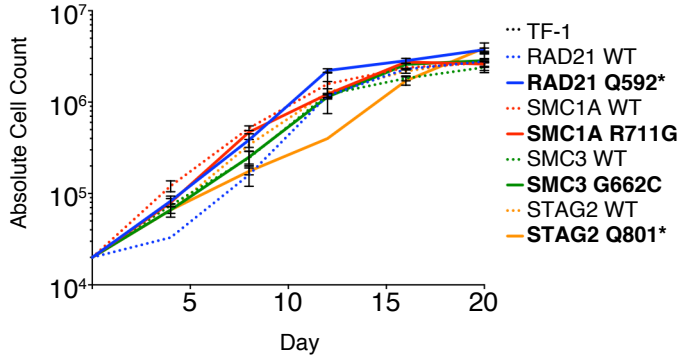

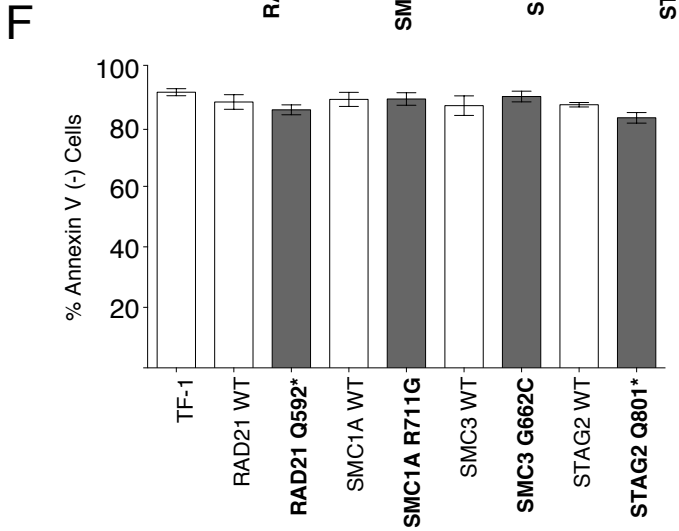

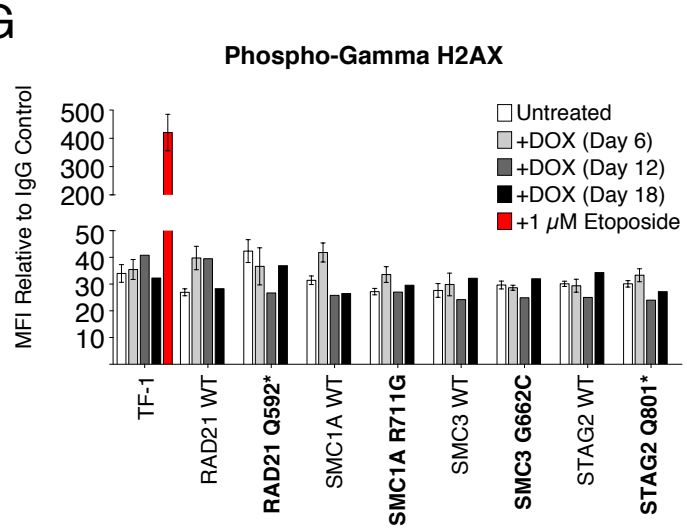

Supplementary Figure 1

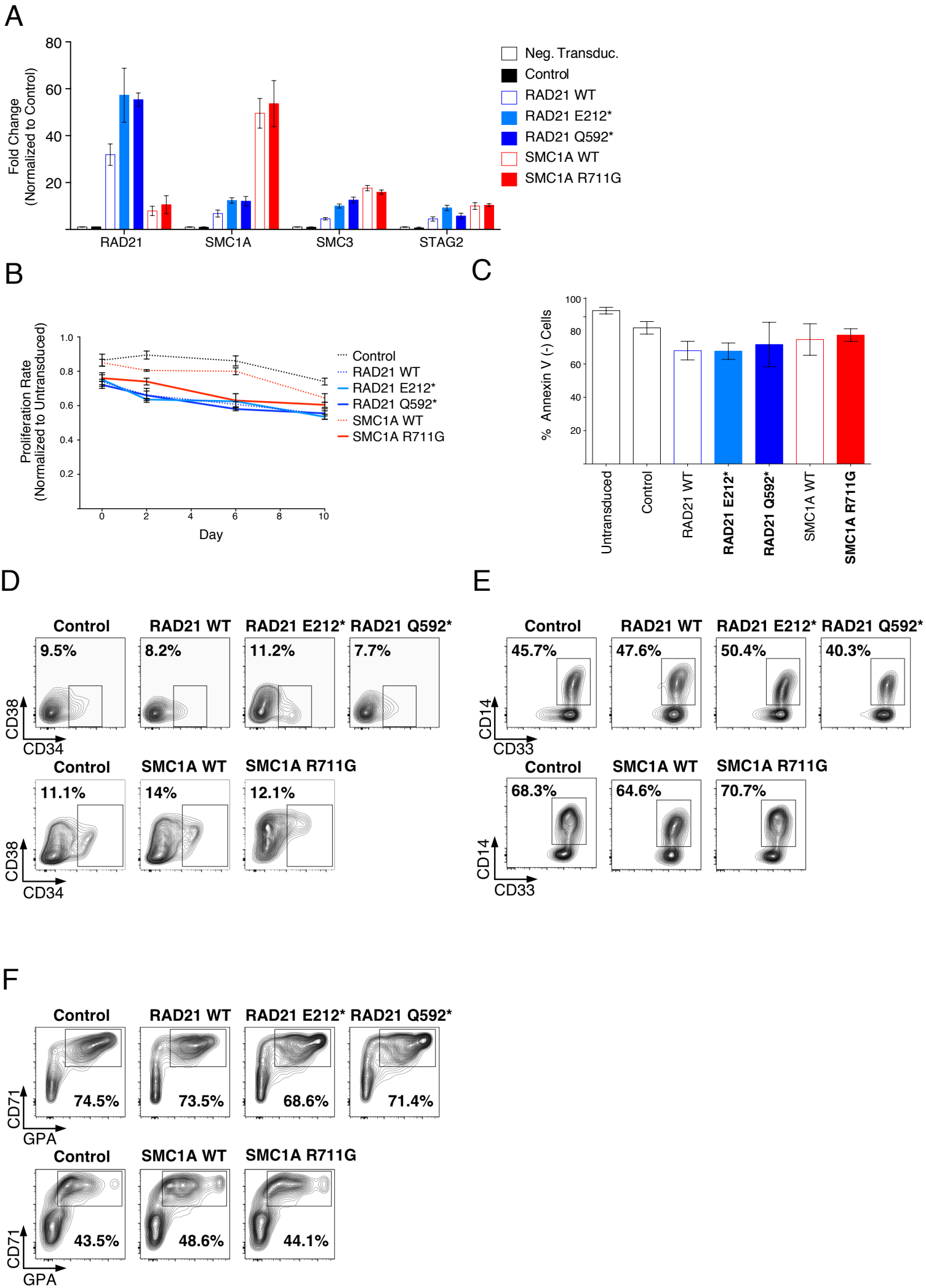

Supplementary Figure 2

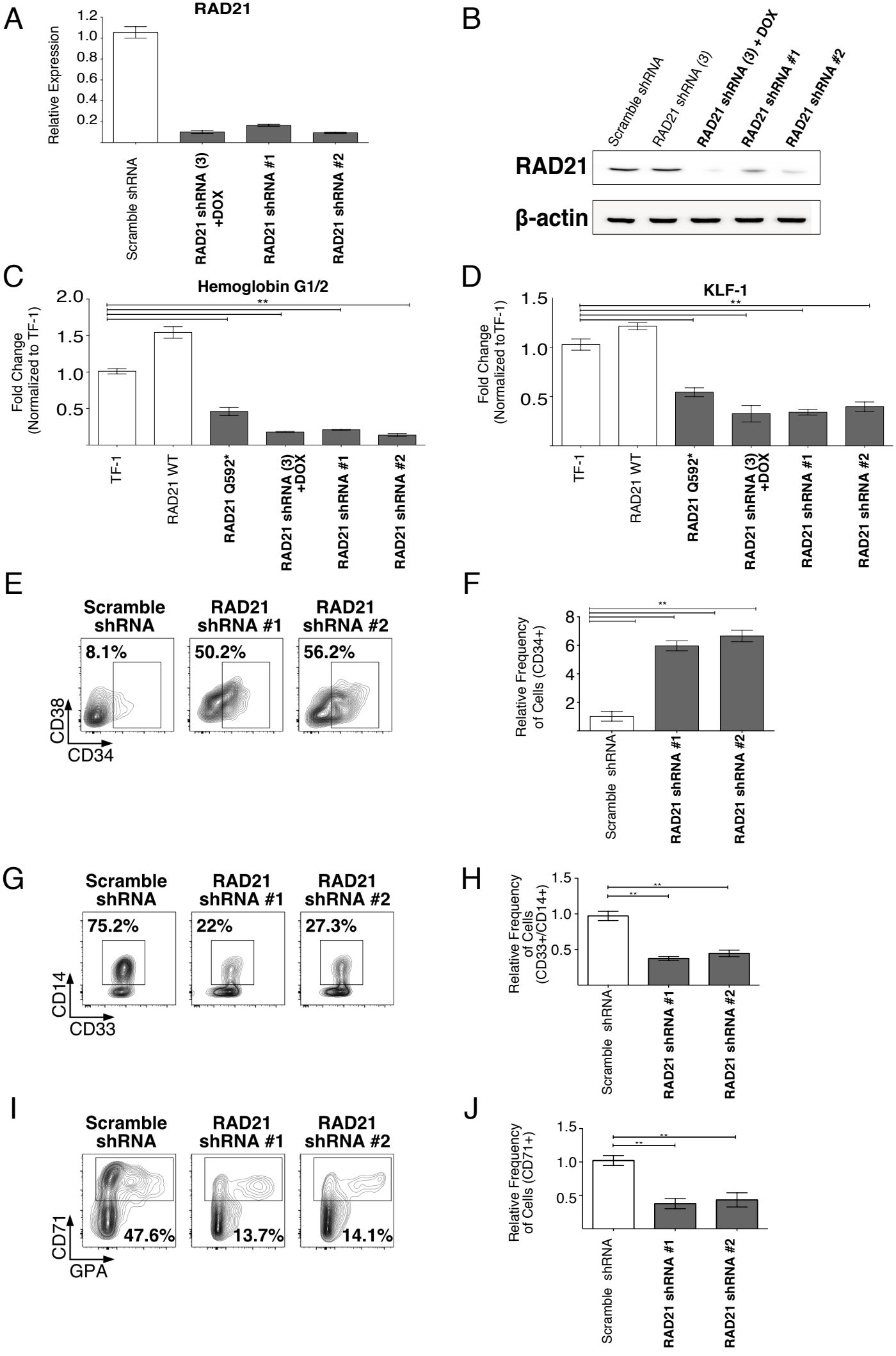

Supplementary Figure 3

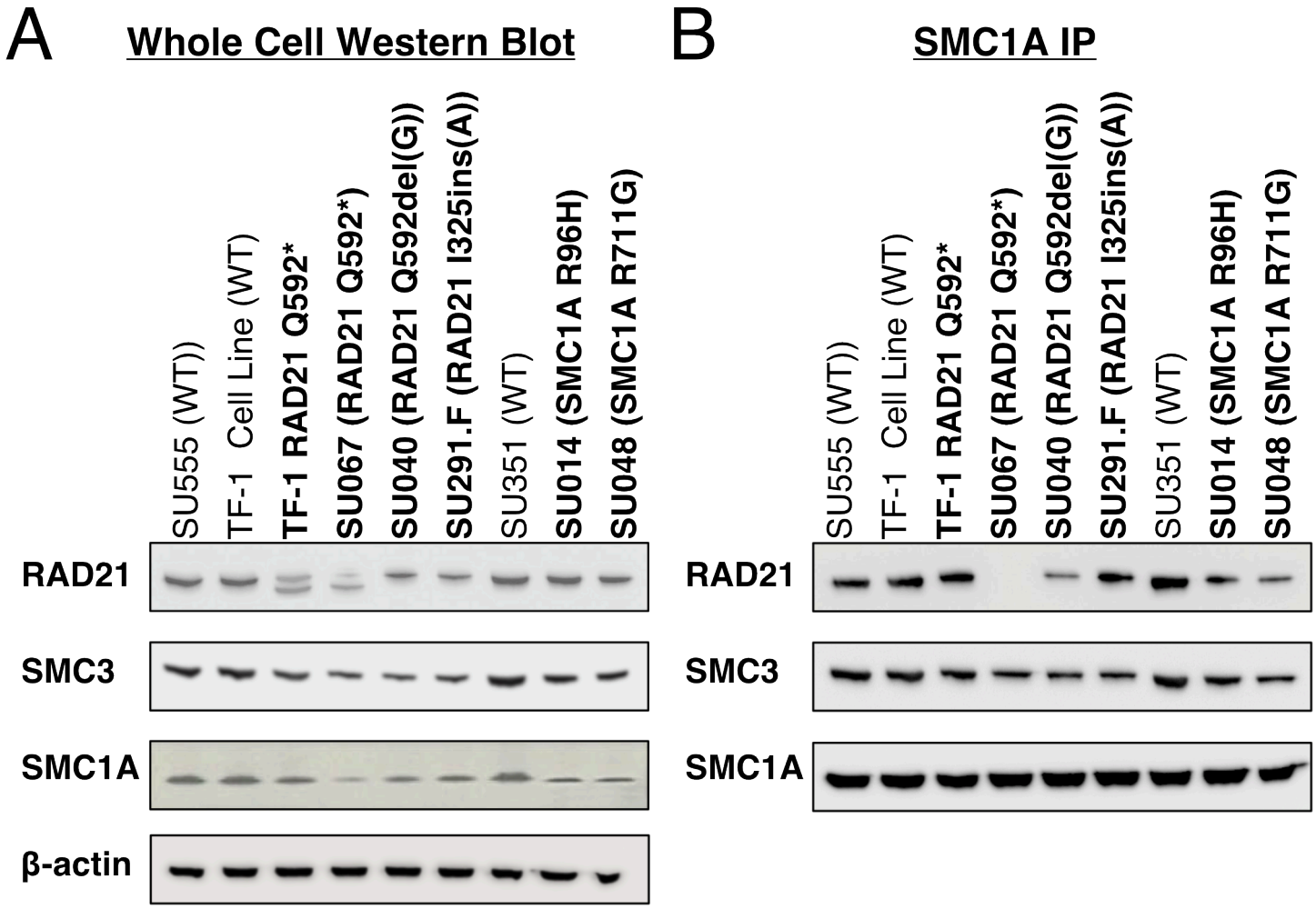

Supplementary Figure 4

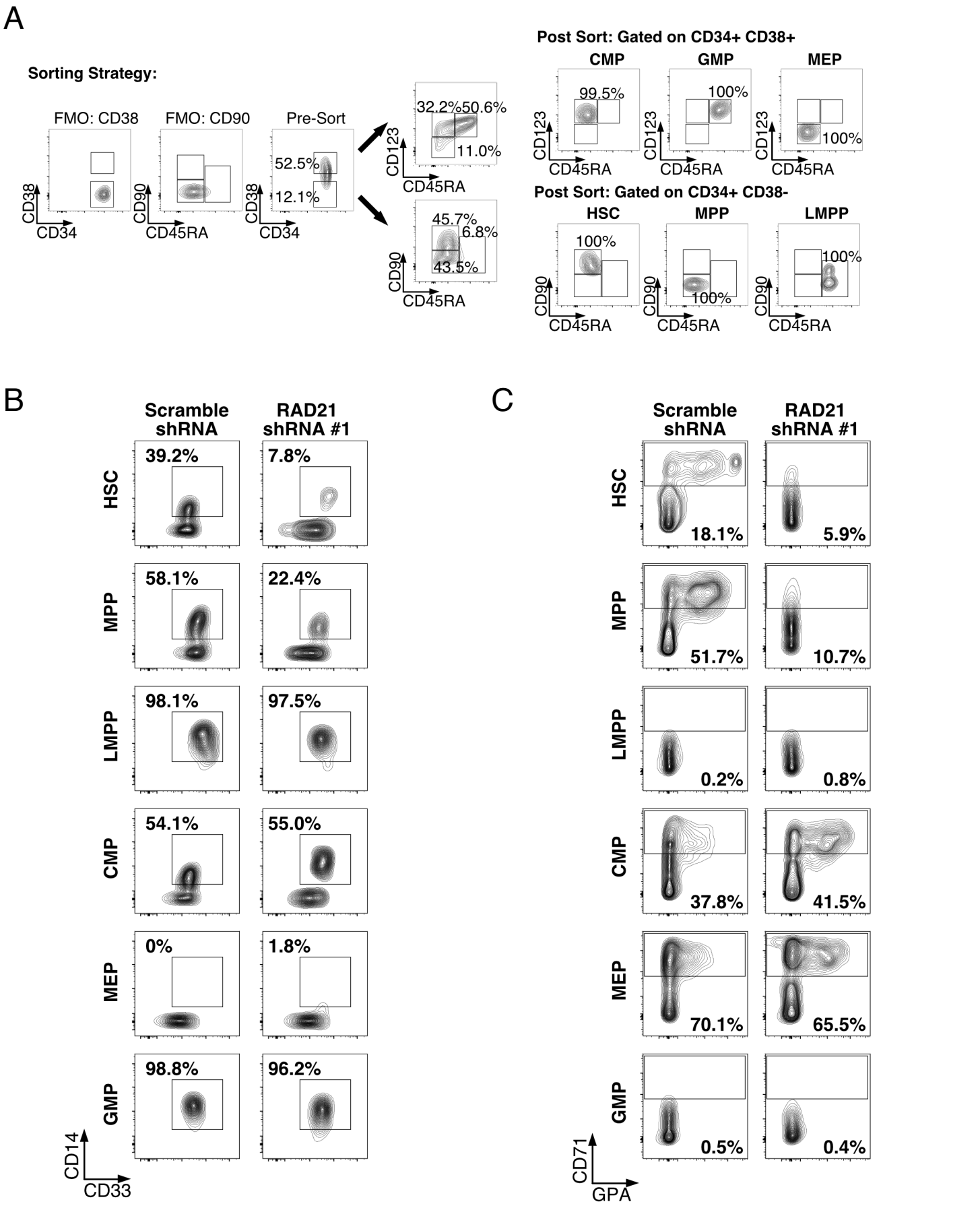

Supplementary Figure 5

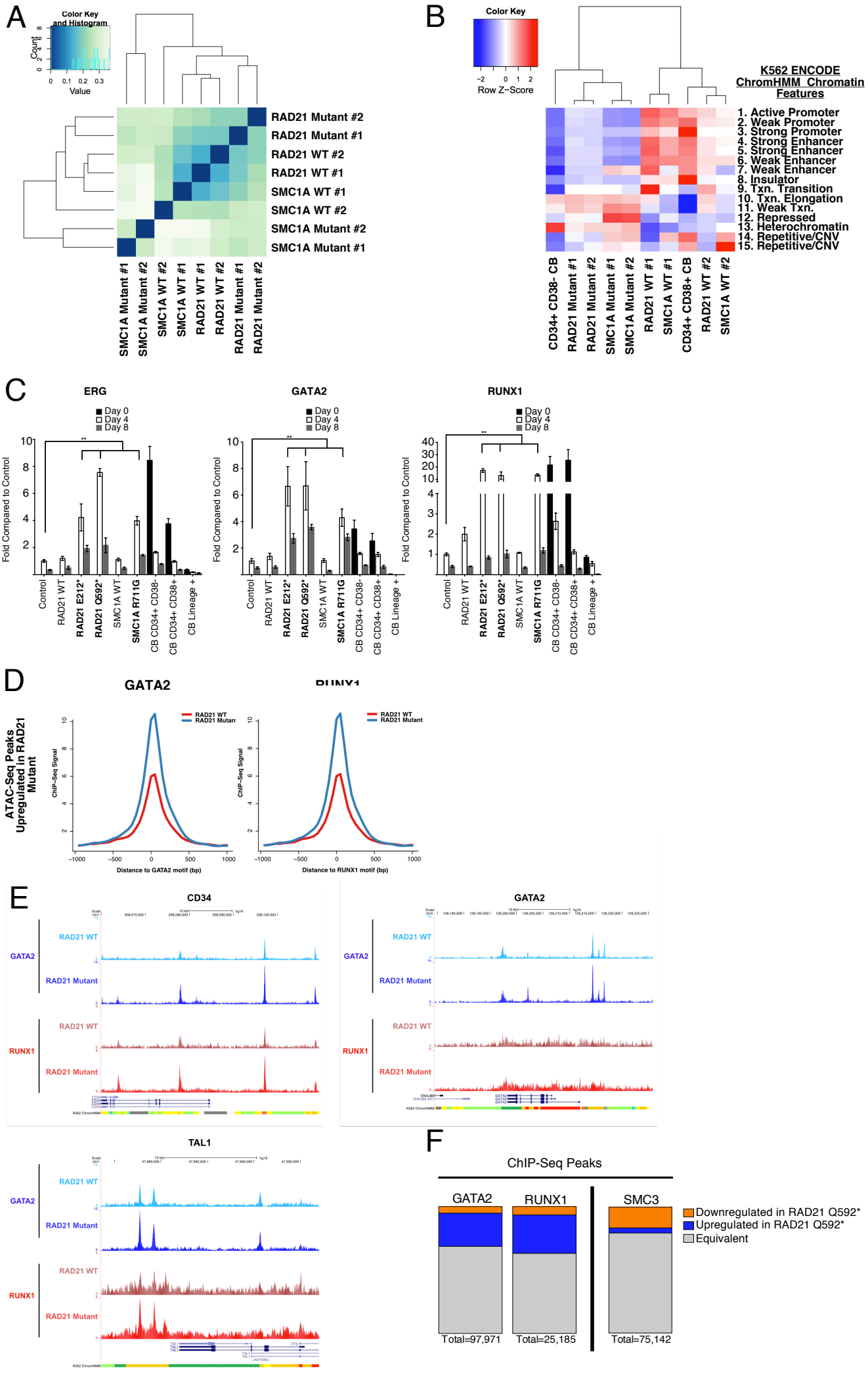
A
Color Key and Histogram
Count
Value
RAD21 Mutant #2
RAD21 Mutant #1
RAD21 WT #2
RAD21 WT #1
SMC1A WT #1
SMC1A WT #2
SMC1A Mutant #2
SMC1A Mutant #1
B
Color Key
Row Z-Score
K562 ENCODE ChromHMM Chromatin Features
1. Active Promoter
2. Weak Promoter
3. Strong Promoter
4. Strong Enhancer
5. Strong Enhancer
6. Weak Enhancer
7. Weak Enhancer
8. Insulator
9. Txn. Transition
10. Txn. Elongation
11. Weak Txn.
12. Repressed
13. Heterochromatin
14. Repetitive/CNV
15. Repetitive/CNV
CD34+ CD38- CB
RAD21 Mutant #1
RAD21 Mutant #2
SMC1A Mutant #1
SMC1A Mutant #2
RAD21 WT #1
SMC1A WT #1
CD34+ CD38+ CB
RAD21 WT #2
SMC1A WT #2
C
ERG
GATA2
RUNX1
Day 0
Day 4
Day 8
Fold Compared to Control
Control
RAD21 WT
RAD21 E212*
RAD21 Q592*
SMC1A WT
SMC1A R711G
CB CD34+ CD38-
CB CD34+ CD38+
CB Lineage +
D
GATA2
RUNX1
ATAC-Seq Peaks Upregulated in RAD21 Mutant
RAD21 WT
RAD21 Mutant
ChIP-Seq Signal
Distance to GATA2 motif (bp)
Distance to RUNX1 motif (bp)
E
CD34
GATA2
TAL1
RAD21 WT
RAD21 Mutant
GATA2
RUNX1
F
ChIP-Seq Peaks
GATA2
RUNX1
SMC3
Total=97,971
Total=25,185
Total=75,142
Downregulated in RAD21 Q592*
Upregulated in RAD21 Q592*
Equivalent

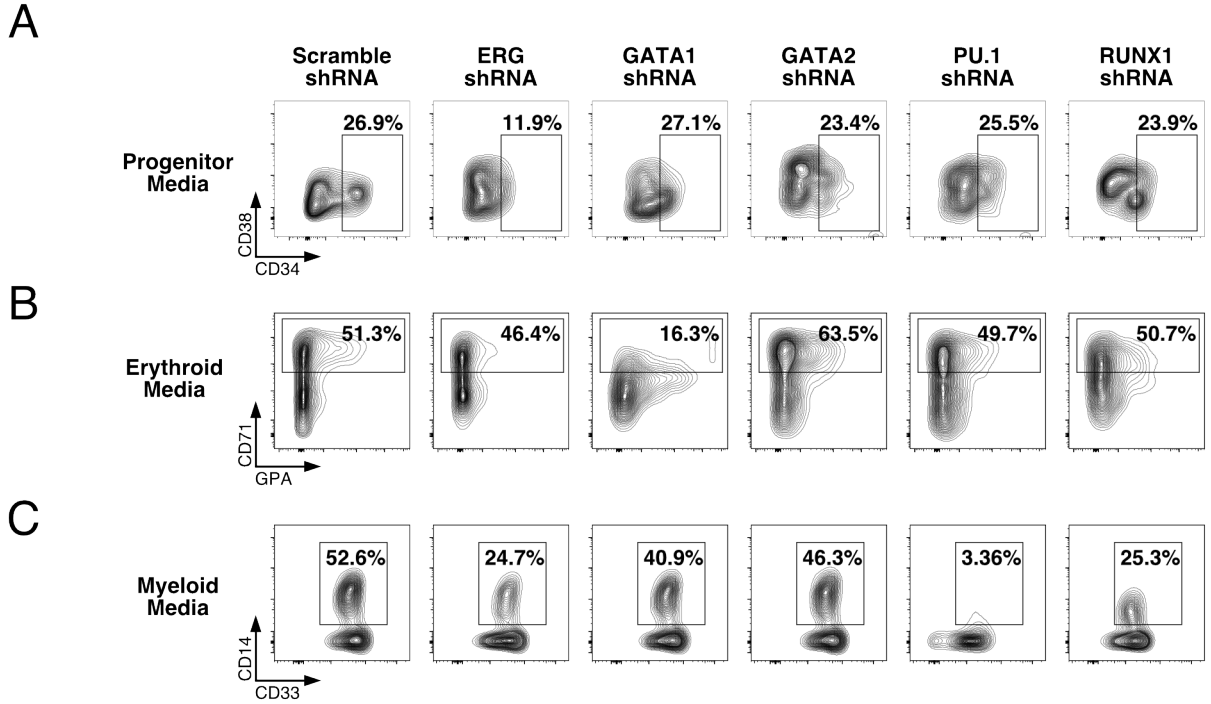

Supplementary Figure 7

Supplementary Table 1: Primary AML Sample Information							
Sample	**Disease Type**	**WHO Classification**	**Cytogenetics**	**Age**	**Gender**	**Cohesin Status**	**Other Mutations**
SU014	De Novo	AML not-otherwise specified	Normal	59	M	SMC1A Mutant (R96H)	IDH1-R132H, NPM1-L287ins(TCTG), ZBTB33-C496Y, FLT3-ITD
SU040	De Novo	AML not-otherwise specified	Normal	57	F	RAD21 Mutant (Q592del(G))	DNMT3A-R882H, BRWD3-R1447Q, MTCO1-A387T, FLT3-N841K, NPM1-L287ins(TCTG)
SU048	De Novo	AML not-otherwise specified	Normal	76	F	SMC1A Mutant (R711G)	TET2-E1357*, TET2-D1384V, NPM1-L287ins(TCTG), FLT3-ITD
SU067	De Novo	AML not-otherwise specified	Normal	54	F	RAD21 Mutant (Q592*)	PTPN11-A72T, NPM1-L287ins(TCTG)
SU291.F	Relapse	AML not-otherwise specified	+8	38	F	RAD21 Mutant (I325ins(A))	IDH1-R132H, FLT3-D835Y, SMG1-V2264I, , NPM1-L287ins(TCTG), DNMT3A-S535ins(21bp)
SU351	De Novo	AML with multilineage dysplasia without antecedent MDS	der(10)t(X;10),+8	75	M	Cohesin WT	IDH2-R140Q, NRAS-G13V, SI-R250H, BCORL1-G121R, SETD2-D2100H, SETD2-T2101del(A)
SU555	De Novo	AML not-otherwise specified	Normal	27	F	Cohesin WT	MTND6-T19I, LRP1B-I2264V, MTND4-L65P, PTPN11-G60V, SETD2-T2540ins(AA)

Supplementary Table 3: Top 50 Motifs Upregulated in ATAC-Seq Data			
	Upregulated in TF-1 RAD21 Q592* vs. RAD21 WT	**Upregulated in Human Cord Blood RAD21 Mutant vs. RAD21 WT**	**Upregulated in Human Cord Blood SMC1A Mutant vs. SMC1A WT**
1	Gata1(Zf)/K562-GATA1-ChIP-Seq(GSE18829)/Homer	Gata2(Zf)/K562-GATA2-ChIP-Seq/Homer	ERG(ETS)/VCaP-ERG-ChIP-Seq/Homer
2	Gata2(Zf)/K562-GATA2-ChIP-Seq(GSE18829)/Homer	Gata1(Zf)/K562-GATA1-ChIP-Seq/Homer	Fli1(ETS)/CD8-FLI-ChIP-Seq(GSE20898)/Homer
3	Gata4(Zf)/Heart-Gata4-ChIP-Seq(GSE35151)/Homer	Gata4(Zf)/Heart-Gata4-ChIP-Seq(GSE35151)/Homer	ETV1(ETS)/GIST48-ETV1-ChIP-Seq/Homer
4	CTCF(Zf)/CD4+-CTCF-ChIP-Seq(Barski et al.)/Homer	ERG(ETS)/VCaP-ERG-ChIP-Seq/Homer	ETS1(ETS)/Jurkat-ETS1-ChIP-Seq/Homer
5	Fli1(ETS)/CD8-FLI-ChIP-Seq(GSE20898)/Homer	GATA3(Zf)/iTreg-Gata3-ChIP-Seq(GSE20898)/Homer	EWS:ERG-fusion(ETS)/CADO_ES1-EWS:ERG-ChIP-Seq/Homer
6	ETV1(ETS)/GIST48-ETV1-ChIP-Seq(GSE22441)/Homer	ETV1(ETS)/GIST48-ETV1-ChIP-Seq/Homer	CTCF(Zf)/CD4+-CTCF-ChIP-Seq/Homer
7	ETS1(ETS)/Jurkat-ETS1-ChIP-Seq(GSE17954)/Homer	ETS1(ETS)/Jurkat-ETS1-ChIP-Seq/Homer	PU.1(ETS)/ThioMac-PU.1-ChIP-Seq/Homer
8	GATA:SCL/Ter119-SCL-ChIP-Seq(GSE18720)/Homer	Fli1(ETS)/CD8-FLI-ChIP-Seq(GSE20898)/Homer	GABPA(ETS)/Jurkat-GABPa-ChIP-Seq/Homer
9	GATA3(Zf)/iTreg-Gata3-ChIP-Seq(GSE20898)/Homer	RUNX1(Runt)/Jurkat-RUNX1-ChIP-Seq/Homer	Ets1-distal(ETS)/CD4+-PolII-ChIP-Seq/Homer
10	GABPA(ETS)/Jurkat-GABPa-ChIP-Seq(GSE17954)/Homer	RUNX(Runt)/HPC7-Runx1-ChIP-Seq/Homer	EWS:FLI1-fusion(ETS)/SK_N_MC-EWS:FLI1-ChIP-Seq/Homer
11	ERG(ETS)/VCaP-ERG-ChIP-Seq(GSE14097)/Homer	EWS:ERG-fusion(ETS)/CADO_ES1-EWS:ERG-ChIP-Seq/Homer	Gata1(Zf)/K562-GATA1-ChIP-Seq/Homer
12	BORIS(Zf)/K562-CTCFL-ChIP-Seq(GSE32465)/Homer	GABPA(ETS)/Jurkat-GABPa-ChIP-Seq/Homer	Gata2(Zf)/K562-GATA2-ChIP-Seq/Homer
13	ELF5(ETS)/T47D-ELF5-ChIP-Seq(GSE30407)/Homer	RUNX2(Runt)/PCa-RUNX2-ChIP-Seq(GSE33889)/Homer	BORIS(Zf)/K562-CTCFL-ChIP-Seq/Homer
14	PU.1(ETS)/ThioMac-PU.1-ChIP-Seq(GSE21512)/Homer	EWS:FLI1-fusion(ETS)/SK_N_MC-EWS:FLI1-ChIP-Seq/Homer	Gata4(Zf)/Heart-Gata4-ChIP-Seq(GSE35151)/Homer
15	EHF(ETS)/LoVo-EHF-ChIP-Seq(GSE49402)/Homer	Ets1-distal(ETS)/CD4+-PolII-ChIP-Seq/Homer	RUNX1(Runt)/Jurkat-RUNX1-ChIP-Seq/Homer
16	Ets1-distal(ETS)/CD4+-PolII-ChIP-Seq(Barski et al.)/Homer	RUNX-AML(Runt)/CD4+-PolII-ChIP-Seq/Homer	RUNX(Runt)/HPC7-Runx1-ChIP-Seq/Homer
17	ELF1(ETS)/Jurkat-ELF1-ChIP-Seq(SRA014231)/Homer	PU.1(ETS)/ThioMac-PU.1-ChIP-Seq/Homer	RUNX-AML(Runt)/CD4+-PolII-ChIP-Seq/Homer
18	Elk4(ETS)/Hela-Elk4-ChIP-Seq(GSE31477)/Homer	GATA:SCL/Ter119-SCL-ChIP-Seq/Homer	ETS:E-box/HPC7-Scl-ChIP-Seq/Homer
19	Elk1(ETS)/Hela-Elk1-ChIP-Seq(GSE31477)/Homer	Jun-AP1(bZIP)/K562-cJun-ChIP-Seq/Homer	RUNX2(Runt)/PCa-RUNX2-ChIP-Seq(GSE33889)/Homer
20	ETS(ETS)/Promoter/Homer	HIF1b(HLH)/O785-HIF1b-ChIP-Seq(GSE34871)/Homer	GATA3(Zf)/iTreg-Gata3-ChIP-Seq(GSE20898)/Homer
21	EWS:FLI1-fusion(ETS)/SK_N_MC-EWS:FLI1-ChIP-Seq(SRA014231)/Homer	AP-1(bZIP)/ThioMac-PU.1-ChIP-Seq/Homer	Jun-AP1(bZIP)/K562-cJun-ChIP-Seq/Homer
22	EWS:ERG-fusion(ETS)/CADO_ES1-EWS:ERG-ChIP-Seq(SRA014231)/Homer	Atoh1(bHLH)/Cerebellum-Atoh1-ChIP-Seq/Homer	AP-1(bZIP)/ThioMac-PU.1-ChIP-Seq/Homer
23	Jun-AP1(bZIP)/K562-cJun-ChIP-	CTCF(Zf)/CD4+-CTCF-ChIP-	HIF1b(HLH)/O785-HIF1b-ChIP-

	Seq(GSE31477)/Homer	Seq/Homer	Seq(GSE34871)/Homer
24	BATF(bZIP)/Th17-BATF-ChIP-Seq(GSE39756)/Homer	ELF1(ETS)/Jurkat-ELF1-ChIP-Seq/Homer	SPDEF(ETS)/VCaP-SPDEF-ChIP-Seq/Homer
25	Atf3(bZIP)/GBM-ATF3-ChIP-Seq(GSE33912)/Homer	Elk4(ETS)/Hela-Elk4-ChIP-Seq(GSE31477)/Homer	GATA:SCL/Ter119-SCL-ChIP-Seq/Homer
26	AP-1(bZIP)/ThioMac-PU.1-ChIP-Seq(GSE21512)/Homer	NeuroD1(bHLH)/Islet-NeuroD1-ChIP-Seq(GSE30298)/Homer	ETS(ETS)/Promoter/Homer
27	RUNX(Runt)/HPC7-Runx1-ChIP-Seq(GSE22178)/Homer	Elk1(ETS)/Hela-Elk1-ChIP-Seq(GSE31477)/Homer	ELF1(ETS)/Jurkat-ELF1-ChIP-Seq/Homer
28	RUNX1(Runt)/Jurkat-RUNX1-ChIP-Seq(GSE29180)/Homer	SPDEF(ETS)/VCaP-SPDEF-ChIP-Seq/Homer	SCL/HPC7-Scl-ChIP-Seq/Homer
29	Bach2(bZIP)/OCILy7-Bach2-ChIP-Seq(GSE44420)/Homer	BORIS(Zf)/K562-CTCFL-ChIP-Seq/Homer	Atoh1(bHLH)/Cerebellum-Atoh1-ChIP-Seq/Homer
30	SPDEF(ETS)/VCaP-SPDEF-ChIP-Seq(SRA014231)/Homer	Bach1(bZIP)/K562-Bach1-ChIP-Seq(GSE31477)/Homer	Elk1(ETS)/Hela-Elk1-ChIP-Seq(GSE31477)/Homer
31	Sp1(Zf)/Promoter/Homer	SCL/HPC7-Scl-ChIP-Seq/Homer	NeuroD1(bHLH)/Islet-NeuroD1-ChIP-Seq(GSE30298)/Homer
32	RUNX-AML(Runt)/CD4+-PolII-ChIP-Seq(Barski et al.)/Homer	ETS:E-box/HPC7-Scl-ChIP-Seq/Homer	Elk4(ETS)/Hela-Elk4-ChIP-Seq(GSE31477)/Homer
33	RUNX2(Runt)/PCa-RUNX2-ChIP-Seq(GSE33889)/Homer	NF-E2(bZIP)/K562-NFE2-ChIP-Seq/Homer	NF-E2(bZIP)/K562-NFE2-ChIP-Seq/Homer
34	BMYB(HTH)/Hela-BMYB-ChIPSeq(GSE27030)/Homer	Nrf2(bZIP)/Lymphoblast-Nrf2-ChIP-Seq(GSE37589)/Homer	ETS:RUNX/Jurkat-RUNX1-ChIP-Seq/Homer
35	MYB(HTH)/ERMYB-Myb-ChIPSeq(GSE22095)/Homer	Tcf12(HLH)/GM12878-Tcf12-ChIP-Seq/Homer	Bach1(bZIP)/K562-Bach1-ChIP-Seq(GSE31477)/Homer
36	AMYB(HTH)/Testes-AMYB-ChIP-Seq(GSE44588)/Homer	ETS(ETS)/Promoter/Homer	Nrf2(bZIP)/Lymphoblast-Nrf2-ChIP-Seq(GSE37589)/Homer
37	NFY(CCAAT)/Promoter/Homer	MyoD(HLH)/Myotube-MyoD-ChIP-Seq/Homer	Olig2(bHLH)/Neuron-Olig2-ChIP-Seq(GSE30882)/Homer
38	Bach1(bZIP)/K562-Bach1-ChIP-Seq(GSE31477)/Homer	Olig2(bHLH)/Neuron-Olig2-ChIP-Seq(GSE30882)/Homer	Foxo1(Forkhead)/RAW-Foxo1-ChIP-Seq/Homer
39	NF-E2(bZIP)/K562-NFE2-ChIP-Seq(GSE31477)/Homer	MyoG(HLH)/C2C12-MyoG-ChIP-Seq(GSE36024)/Homer	Hoxc9/Ainv15-Hoxc9-ChIP-Seq/Homer
40	ETS:RUNX/Jurkat-RUNX1-ChIP-Seq(GSE17954)/Homer	ETS:RUNX/Jurkat-RUNX1-ChIP-Seq/Homer	Tcf12(HLH)/GM12878-Tcf12-ChIP-Seq/Homer
41	Nrf2(bZIP)/Lymphoblast-Nrf2-ChIP-Seq(GSE37589)/Homer	Myf5(bHLH)/GM-Myf5-ChIP-Seq(GSE24852)/Homer	MyoG(HLH)/C2C12-MyoG-ChIP-Seq(GSE36024)/Homer
42	GFY-Staf/Promoters/Homer	MYB(HTH)/ERMYB-Myb-ChIPSeq(GSE22095)/Homer	MyoD(HLH)/Myotube-MyoD-ChIP-Seq/Homer
43	KLF5(Zf)/LoVo-KLF5-ChIP-Seq(GSE49402)/Homer	BMYB(HTH)/Hela-BMYB-ChIPSeq(GSE27030)/Homer	REST-NRSF(Zf)/Jurkat-NRSF-ChIP-Seq/Homer
44	SCL(HLH)/HPC7-Scl-ChIP-Seq(GSE13511)/Homer	EGR(Zf)/K562-EGR1-ChIP-Seq/Homer	PU.1-IRF/Bcell-PU.1-ChIP-Seq/Homer
45	PU.1-IRF(ETS:IRF)/Bcell-PU.1-ChIP-Seq(GSE21512)/Homer	Hoxc9/Ainv15-Hoxc9-ChIP-Seq/Homer	BMYB(HTH)/Hela-BMYB-ChIPSeq(GSE27030)/Homer
46	Stat3+il21(Stat)/CD4-Stat3-ChIP-Seq(GSE19198)/Homer	MafK(bZIP)/C2C12-MafK-ChIP-Seq(GSE36030)/Homer	HOXA9/HSC-Hoxa9-ChIP-Seq(GSE33509)/Homer
47	STAT4(Stat)/CD4-Stat4-ChIP-Seq(GSE22104)/Homer	MafA(bZIP)/Islet-MafA-ChIP-Seq(GSE30298)/Homer	MafK(bZIP)/C2C12-MafK-ChIP-Seq(GSE36030)/Homer
48	GFY(?)/Promoter/Homer	STAT4(Stat)/CD4-Stat4-ChIP-Seq/Homer	MafA(bZIP)/Islet-MafA-ChIP-Seq(GSE30298)/Homer
49	Maz(Zf)/HepG2-Maz-ChIP-Seq(GSE31477)/Homer	Foxo1(Forkhead)/RAW-Foxo1-ChIP-Seq/Homer	Myf5(bHLH)/GM-Myf5-ChIP-Seq(GSE24852)/Homer
50	Stat3(Stat)/mES-Stat3-ChIP-Seq(GSE11431)/Homer	GATA-IR4(Zf)/iTreg-Gata3-ChIP-Seq(GSE20898)/Homer	RFX(HTH)/K562-RFX3-ChIP-Seq/Homer